Journal of The Electrochemical Society, **161** (5) A682-A692 (2014)
0013-4651/2014/161(5)/A682/11/$31.00 © The Electrochemical Society

Lithium Intercalation in Core-Shell Materials–Theoretical Analysis

Bharatkumar Suthar* **and Venkat R. Subramanian**,z**

Department of Energy, Environmental and Chemical Engineering, Washington University, St. Louis, Missouri 63130, USA

Core-shell composite structures are potential candidates for Li-ion battery electrodes as they can take advantage of materials with higher energy density and materials with higher cyclability. This paper derives an analytical solution for isotropic 1-dimensional diffusion with galvanostatic boundary condition in composite slab, cylinder and sphere using separation of variables method. A general interfacial condition has been used to represent the dynamics at the interface of the composite material rendering the solution useful for wide variety of battery materials. Using the derived analytical solution for diffusion, intercalation induced stresses were estimated for spherical core-shell materials.

Manuscript submitted January 13, 2014; revised manuscript received February 19, 2014. Published March 11, 2014.

Lithium-ion chemistries are attractive for many applications due to high cell voltage, high volumetric and gravimetric energy density (100 Wh/kg), high power density (300 W/kg), good temperature range, low memory effect, and relatively long battery life.[1–3] Capacity fade, underutilization, and thermal runaway are the main issues that need to be addressed in order to use a lithium-ion battery efficiently and safely for a long life.

In order to meet energy demands and address environmental concerns, researchers are actively working on novel energy storage materials of which a significant fraction is dedicated to developing insertion materials for lithium ion batteries.[4–6] One way to achieve higher energy densities in lithium ion batteries is by replacing currently used graphite (theoretical storage capacity of 372 mAh/g) based anode with materials like silicon (theoretical storage capacity of 4200 mAh/g). While materials such as silicon and tin have high energy density compared to graphite, they suffer from high volumetric expansion (∼400%) during intercalation/deintercalation which results into pulverization and electrical isolation of the electrode materials. A change in volume of such magnitude causes delamination of the solid electrolyte interface (SEI) from the active material. Delamination and formation of new SEI layer at the exposed surface continuously consumes active materials resulting in faster capacity fade.[7] One way to take advantage of higher energy density materials is to develop core –shell composite materials where the shell materials have more favorable mechanical properties than the core. To our knowledge, intercalation in core-shell materials has not been modeled and reported in the literature. Previous efforts by Subramanian and White[8] only included analysis of composite materials with two different diffusivities. However, if two different materials are used in core-shell configuration, interfacial dynamics cannot be ignored.

Subramanian and White[8] derived analytical solution under galvanostatic conditions for composite materials having concentration and flux continuity at the interface. This paper extends the method adopted by Subramanian and White[8] for a general treatment at the interface of composite materials in order to make it useful for a wide variety of materials and configurations (e.g. core-shell configuration with flexibility of electrochemically active and inert core, hollow materials, etc.). We derive and present an analytical solution for isotropic diffusion in 1-dimension for rectangular, cylindrical and spherical core-shell particles. The results reported here can be used for core-shell or hollow materials with low volumetric expansion. Materials with large volume changes cannot be addressed directly using the analytical solution reported in this paper. However, the interfacial boundary condition introduced in this paper is valid for any core-shell type electrode material. Moving boundary formulation should be considered to simulate diffusion in high volume expansion materials which will require numerical treatment.

Section 2 gives a brief introduction to the diffusion problem in composite materials and intercalation induced stresses. Section 3 presents the solution methodology using the separation of variables approach for planar geometry and lists solutions for cylinder and sphere. Intercalation dynamics for several sets of transport parameters are presented in section 4. Section 5 illustrates the use of analytical solution for diffusion in quantifying intercalation induced stresses for spherical composite particle followed by code dissemination section. Section 7 presents conclusion and future directions.

Background

Diffusion in heterogeneous media is an extensively studied problem in many branches of engineering. Heat conduction through heterogeneous media is typically studied where temperature is continuous across interfaces.[9] Models for heat and mass transfer in biological tissues result in similar problems with discontinuous interface conditions.[10,11] Subramanian and White[8] presented analytical solution for composite material for galvanostatic boundary conditions with continuous concentration and flux at the interface. To our knowledge, none of the previous work considers the problem of diffusion in heterogeneous media with inhomogeneous boundary condition (constant flux arising from galvanostatic boundary condition at the surface where the electrochemical reaction occurs) and discontinuous interfacial concentration with associated kinetics, which is of the practical importance for novel composite battery materials. We consider the problem of diffusion in heterogeneous media composed of two different materials with different transport properties (diffusion coefficients, D_i) and associated interfacial dynamics (Figure 1).

Diffusion in composites with two materials can be classified into 4 possible scenarios depending on the ratio of diffusivity and equilibrium concentration (Figure 2). Cases A ($D_2/D_1 > 1$) and B ($D_2/D_1 < 1$) in Figure 2 with $c_1^*/c_2^* < 1$, are very similar to the diffusion in sphere with single domain where the concentration in the inner core will always be smaller compared to the outer shell during

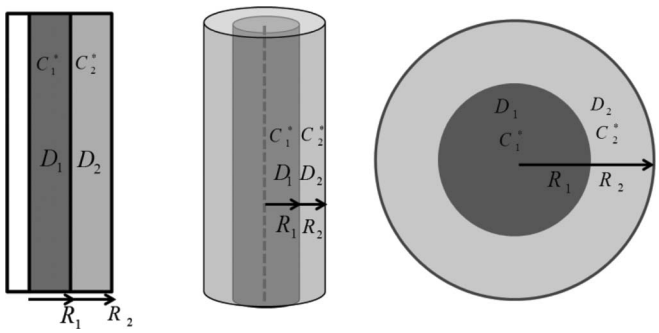

Figure 1. Composite geometries under consideration.

*Electrochemical Society Student Member.
**Electrochemical Society Active Member.
zE-mail: vsubramanian@seas.wustl.edu

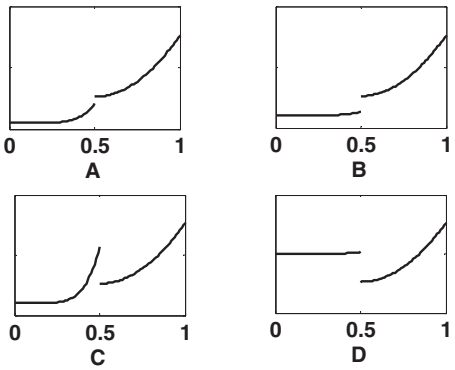

Figure 2. 4 possible diffusion dynamics in 2-region composite geometry.

intercalation. Interesting diffusion dynamics are observed in cases C ($D_2/D_1 > 1$) and D ($D_2/D_1 < 1$) with $c_1^*/c_2^* > 1$ which may cause the inner core of the particle to become more concentrated than the other shell.

In order to quantify the intercalation induced stresses for the four cases above, even the very basic treatment of stress will require three additional material properties: Young's modulus, Poisson's ratio and partial molar volume. Using a thermal analogy model for intercalation induced stresses assuming concentration independent material properties and ignoring volume expansion, decoupling of concentration and stress is possible.[12–16] Having all the parameters (diffusivity, equilibrium concentration, thickness, Young's modulus, Poisson's ratio, and partial molar volume) in a unified analytical framework to quantify stress will help guide the design of next generation energy storage materials.

Model and Solution Methodology

Considering unsteady state diffusion, a material balance yields the following equation for concentration.

$$\frac{\partial c_i}{\partial t} = -\nabla . N_i \qquad [1]$$

Here $i = 1$ and 2 for region 1 and region 2, c_i is the concentration (mol/m^3), t is time (s) and N_i is molar flux (mol/s/m^2) which can be treated according to Fick's laws as

$$N_i = -D_i \nabla C_i \qquad [2]$$

where D_i is diffusion coefficient (m^2/s). For simplicity, the model and method are illustrated for planar geometry. Assuming constant diffusivity and considering 1-dimensional diffusion of lithium for planar geometry, Eq. 1 can be written as

$$\frac{\partial c_i}{\partial t} = D_i \frac{\partial^2 c_i}{\partial r^2} \qquad [3]$$

where r is axial distance (m). Transient diffusion in composite planar sheet consisting of two regions of different thicknesses and different diffusion coefficients (as described in Figure 1) can be described using the following equations

$$\frac{\partial}{\partial t} c_1 (r, t) = D_1 \frac{\partial^2}{\partial r^2} c_1 (r, t), \quad 0 < r < R_1 \qquad [4]$$

$$\frac{\partial}{\partial t} c_2 (r, t) = D_2 \frac{\partial^2}{\partial r^2} c_2 (r, t), \quad R_1 < r < R_2 \qquad [5]$$

where R_1 is the thickness of first region and $R_2 - R_1$ is the thickness of second region, D_1 and D_2 are the diffusion coefficients of the two regions. Initially both the regions are considered empty, i.e. species concentration is zero.

$$c_1 (r, 0) = 0, \quad c_2 (r, 0) = 0 \text{ for all } r \qquad [6]$$

Symmetry boundary condition (zero flux) can be used at the center

$$-D_1 \frac{\partial}{\partial r} c_1 (0, t) = 0, \quad t > 0 \qquad [7]$$

and galvanostatic boundary condition is considered at the surface ($r = R_2$) where electrochemical intercalation and de-intercalation of lithium occurs.

$$-D_2 \frac{\partial}{\partial r} c_2 (R_2, t) = \frac{I_s}{nF}, \quad t > 0 \qquad [8]$$

Here, I_s is the current density (A/m^2) which is a constant in case of galvanostatic charge/discharge condition, F is the Faraday's constant and n is the charge associated with the single ion of guest molecule (1 in case of lithium ion). At the interface ($r = R_1$) between two regions, flux continuity condition is used.

$$-D_1 \frac{\partial}{\partial r} c_1 (R_1, t) = -D_2 \frac{\partial}{\partial r} c_2 (R_1, t), \quad t > 0 \qquad [9]$$

For the other boundary condition at the interface, Subramanian and White[8] considered continuity in concentration. This paper considers a more general boundary condition which is relevant for core-shell composite materials having different capacities for lithium ions. Difference in interfacial concentration ($c_1 - \kappa c_2$) is related to the local flux,[10,11] where κ is the ratio of equilibrium concentration (c_1^*/c_2^*).

$$D_1 \frac{\partial}{\partial r} c_1 (R_1, t) = \ell \left[c_1 (R_1, t) - \kappa c_2 (R_1, t) \right], \quad t > 0 \qquad [10]$$

where ℓ represents interfacial dynamics (m/s). Introducing dimensionless variables

$$x_1 = \frac{c_1}{c_0}; \; x_2 = \frac{c_2}{c_0}; \; X = \frac{r}{R_2}; \; \tau = t \Big/ \left(\frac{R_2^2}{D_2} \right) \qquad [11]$$

and the dimensionless parameters

$$\beta^2 = \frac{D_2}{D_1}; \; \alpha = \frac{R_1}{R_2}; \; \gamma = \frac{\ell R_2}{D_1}; \; \delta = \frac{I_s R_2}{D_2 n F c_0} \qquad [12]$$

The equations governing transport of lithium can be represented in the following nondimensional forms

$$\frac{\partial}{\partial \tau} x_1 (X, \tau) = \frac{1}{\beta^2} \frac{\partial^2}{\partial X^2} x_1 (X, \tau), \quad 0 < X < \alpha \qquad [13]$$

$$\frac{\partial}{\partial \tau} x_2 (X, \tau) = \frac{\partial^2}{\partial X^2} x_2 (X, \tau), \quad \alpha < X < 1 \qquad [14]$$

with initial and boundary conditions

$$x_1 (X, 0) = x_2 (X, 0) = 0 \text{ for all } X \qquad [15]$$

$$\frac{\partial}{\partial X} x_1 (0, \tau) = 0, \quad \tau > 0 \qquad [16]$$

$$\frac{\partial}{\partial X} x_2 (1, \tau) = -\delta, \quad \tau > 0 \qquad [17]$$

$$\frac{\partial}{\partial X} x_1 (\alpha, \tau) = \gamma \left(x_1 (\alpha, \tau) - \kappa x_2 (\alpha, \tau) \right), \quad \tau > 0 \qquad [18]$$

$$\frac{\partial}{\partial X} x_1 (\alpha, \tau) = \beta^2 \frac{\partial}{\partial X} x_2 (\alpha, \tau), \quad \tau > 0 \qquad [19]$$

Extending the methodology adopted by Subramanian and White,[8] the following solution is proposed for this problem:

$$x_1 (X, \tau) = g_1 (X, \tau) + w_1 (X) + v_1 (\tau) \qquad [20]$$

$$x_2 (X, \tau) = g_2 (X, \tau) + w_2 (X) + v_2 (\tau) \qquad [21]$$

Let g_1 and g_2 satisfy the homogeneous boundary conditions and remaining terms satisfy the nonhomogeneous boundary conditions.

Boundary conditions (Eqs. 16, 17, 18, and 19) in terms of v_i, w_i and g_i can be written as

$$\frac{\partial}{\partial X} g_1(0,\tau) = 0, \text{ and} \frac{\partial}{\partial X} w_1(0) = 0, \quad \tau > 0 \qquad [22]$$

$$\frac{\partial}{\partial X} g_2(1,\tau) = 0 \text{ and } \frac{\partial}{\partial X} w_2(1) = -\delta, \quad \tau > 0 \qquad [23]$$

$$\frac{\partial}{\partial X} g_1(\alpha,\tau) = \gamma\left(g_1(\alpha,\tau) - \kappa g_2(\alpha,\tau)\right), \text{ and}$$
$$\frac{\partial}{\partial X} w_1(\alpha) = \gamma\left(w_1(\alpha) + v_1(\tau) - \kappa(w_2(\alpha) + v_2(\tau))\right) \quad \tau > 0 \qquad [24]$$

$$\frac{\partial}{\partial X} g_1(\alpha,\tau) = \beta^2 \frac{\partial}{\partial X} g_2(\alpha,\tau), \text{ and } \frac{\partial}{\partial X} w_1(\alpha) = \beta^2 \frac{\partial}{\partial X} w_2(\alpha), \quad \tau > 0 \qquad [25]$$

Substituting Eq. 20 into Eq. 13, the following equation is obtained.

$$\frac{\partial}{\partial \tau} g_1(X,\tau) + \frac{d}{d\tau} v_1(\tau) = \frac{1}{\beta^2}\frac{\partial^2}{\partial X^2} g1(X,\tau) + \frac{1}{\beta^2}\frac{d^2}{dX^2} w_1(X) \qquad [26]$$

As g_1 satisfies the homogeneous part and, v_1 and w_1 satisfy non-homogeneous parts, the following equations can be extracted from Eq. 26.

$$\frac{d}{d\tau} v_1(\tau) = \frac{1}{\beta^2}\frac{d^2}{dX^2} w_1(X) = k_1 \qquad [27]$$

$$\frac{\partial}{\partial \tau} g_1(X,\tau) = \frac{1}{\beta^2}\frac{\partial^2}{\partial X^2} g_1(X,\tau) = -\lambda_1^2 \qquad [28]$$

Here, k_1 and λ_1 are arbitrary constants. Solving Eq. 27 and 28 with boundary condition given by Eq. 22 gives the following solution

$$v_1(\tau) + w_1(X) = \frac{1}{2}\beta^2 k_1 X^2 + k_1\tau + a_1 \qquad [29]$$

$$g_1(X,\tau) = B_1 \cos(\lambda_1 \beta X)\, e^{-\lambda_1^2 \tau} \qquad [30]$$

where a_1 and B_1 are integration constants. Similar equations can be derived for concentration in region 2 using Eq. 23 as boundary condition (using two arbitrary constants, λ_2 and k_2) as.

$$v_2(\tau) + w_2(X) = \frac{1}{2}k_2 X^2 - (\delta + k_2) X + k_2\tau + a_2 \qquad [31]$$

$$g_2(X,\tau) = B_2 \frac{\cos[\lambda_2(X-1)]}{\sin(\lambda_2)} e^{-\lambda_2^2 \tau} \qquad [32]$$

where a_2 and B_2 are integration constants. Eqs. 29, 30, 31, and 32 have eight constants (a_1, a_2, k_1, k_2, λ_1, λ_2, B_1 and B_2) to be determined using the initial condition and remaining boundary conditions at the interface ($X = \alpha$). Using expressions for w_1, w_2, v_1, v_2, g_1, and g_2 (Eqs. 29, 30, 31, and 32) to solve for the interfacial boundary condition given by Eq. 24, gives rise to the following relations

$$\lambda_1 = \lambda_2 = \lambda \qquad [33]$$

$$k_1 = \kappa k_2 \qquad [34]$$

$$-\frac{1}{2}\gamma\kappa k_2\alpha^2 + \gamma\kappa\alpha\delta + \gamma\kappa\alpha k_2 - \gamma\kappa a_2 + \frac{1}{2}\beta^2\gamma k_1\alpha^2 + \gamma a_1 - k_1\alpha = 0 \qquad [35]$$

$$\frac{B_1}{\cos(\alpha\lambda - \lambda)\gamma\beta\kappa} = \frac{B_2}{\sin(\lambda)(\beta\gamma\cos(\lambda\beta\alpha) + \lambda\sin(\lambda\beta\alpha))} = A \qquad [36]$$

constant A is introduced to simplify the expressions. Second boundary condition at the interface (Eq. 25) can be used to obtain the following relation

$$k_1 = \left(1 - \frac{1}{\alpha}\right)k_2 - \frac{\delta}{\alpha} \qquad [37]$$

and the equation for obtaining eigenvalues (λ_n)

$$\frac{-\kappa}{\tan\phi_n} + \frac{\beta}{\tan\theta_n} + \frac{\lambda_n}{\gamma} = 0 \qquad [38]$$

where $\theta_n = \alpha\lambda_n\beta$, $\phi_n = \lambda_n(\alpha - 1)$. The solution takes the form of infinite series

$$x_1(X,\tau) = \sum_{n=1}^{\infty} A_n\gamma\beta\kappa\cos\phi_n\cos(\lambda_n\beta X)\, e^{-\lambda_n^2\tau} + \frac{1}{2}\beta^2 k_1 X^2 + k_1\tau + a_1 \qquad [39]$$

$$x_2(X,\tau) = \sum_{n=1}^{\infty} A_n(\beta\gamma\cos\theta_n + \lambda_n\sin\theta_n)\cos[\lambda_n(X-1)]\, e^{-\lambda_n^2\tau} + \frac{1}{2}k_2 X^2 - (\delta + k_2) X + k_2\tau + a_2 \qquad [40]$$

In order to get one more equation for constants a_1 and a_2, initial conditions are used in integral form as

$$\int_0^{\alpha} x_1(X,0)\, dX + \int_{\alpha}^{1} x_2(X,0)\, dX = 0 \qquad [41]$$

which gives rise to the following equation.

$$(1-\alpha)a_2 + a_1\alpha + \frac{1}{6}(\beta^2\kappa - 1)k_2\alpha^3 + \frac{1}{2}(k_2 + \delta)\alpha^2 - \frac{1}{2}\delta - \frac{1}{3}k_2 = 0 \qquad [42]$$

Eqs. 37 and 34 can be used to solve for k_1 and k_2, while Eqs. 35 and 42 can be used to solve for a_1 and a_2.

$$a_1 = \frac{[(\alpha^3\beta^2 + 3\alpha^3 - 6\alpha^2 + 3\alpha)(\kappa - 1) + 2\alpha^3(1-\beta^2) - 3\alpha^2(1-\beta^2) + 1]\kappa\delta}{6[\alpha(\kappa-1)+1]^2} + \frac{1}{\gamma}\frac{(\alpha-1)\alpha\kappa\delta}{[\alpha(\kappa-1)+1]^2} \qquad [43]$$

$$a_2 = \frac{[6\alpha^3(\kappa-1)^2 - (2\alpha^3\beta^2 - 6\alpha^3 - 3\alpha)(\kappa-1) + 2\alpha^3(1-\beta^2) + 1]\delta}{6[\alpha(\kappa-1)+1]^2} + \frac{1}{\gamma}\frac{\alpha^2\kappa\delta}{[\alpha(\kappa-1)+1]^2} \qquad [44]$$

$$k_1 = \kappa k_2 = -\frac{\kappa\delta}{\alpha(\kappa-1)+1} \qquad [45]$$

For Sturm-Liouville problem of this type where the eigenfunctions are quasi-orthogonal, a constant is required to be multiplied in order to make the resultant system orthogonal. In this case κ serves the purpose.[17] The quasi-orthogonal eigenfunctions for this problem are as follows.

$$f_1(X) = \gamma\beta\kappa\cos\phi_n\cos(\lambda_n\beta X) \qquad [46]$$

$$f_2(X) = (\beta\gamma\cos\theta_n + \lambda_n\sin\theta_n)\cos[\lambda_n(X-1)] \qquad [47]$$

Initial conditions can be used to find the coefficients A_n using κ to make the eigenfunctions orthogonal.

$$\int_0^{\alpha} x_1(X,0)\, f_1(X)\, dX + \kappa\left(\int_0^{\alpha} x_2(X,0)\, f_2(X)\, dX\right) = 0 \qquad [48]$$

The expression for A_n can be expressed as

$$A_n = \frac{2\beta\kappa\delta\cos\theta_n\cos\phi_n}{\chi_1^p\lambda_n\left(\chi_2^p\beta\kappa\cos^2\phi_n - \frac{1}{\gamma^2}\chi_3^p\left(\chi_4^p\right)^2\right)} \qquad [49]$$

using the following relations

$$\chi_1^p = \kappa\gamma\cos\phi_n - \lambda_n\sin\phi_n \quad [50]$$

$$\chi_2^p = \cos\theta_n\sin\theta_n + \theta_n \quad [51]$$

$$\chi_3^p = \cos\phi_n\sin\phi_n + \phi_n \quad [52]$$

$$\chi_4^p = \beta\gamma\cos\theta_n + \lambda_n\sin\theta_n \quad [53]$$

Eqs. 39 and 40 are the analytical solution for diffusion in planar electrode where the constituents are given by Eqs. 38, 43, 44, 45, 49, 50, 51, 52, and 53.

Cylindrical geometry.— The governing equations for composites in non-dimensional form in cylindrical coordinates are

$$\frac{\partial}{\partial\tau}x_1(X,\tau) = \frac{1}{\beta^2}\frac{1}{X}\frac{\partial}{\partial X}\left(X\frac{\partial}{\partial X}x_1(X,\tau)\right), \quad 0 < X < \alpha \quad [54]$$

$$\frac{\partial}{\partial\tau}x_2(X,\tau) = \frac{1}{X}\frac{\partial}{\partial X}\left(X\frac{\partial}{\partial X}x_1(X,\tau)\right), \quad \alpha < X < 1 \quad [55]$$

The initial and boundary conditions in this case can be expressed using Eqs. 6, 7, 8, 9, and 10. Using similar approach, the solution for cylindrical coordinate system can be represented as:

$$x_1(X,\tau) = \sum_{n=1}^{\infty} A_n\chi_2^c J_0(\beta\lambda_n X)\,e^{-\lambda_n^2\tau} + \frac{1}{4}k_1\beta^2X^2 + k_1\tau + a_1 \quad 0 \le X < \alpha \quad [56]$$

$$x_2(X,\tau) = \sum_{n=1}^{\infty} A_n\chi_1^c\lambda_n\left[J_1(\lambda_n)Y_0(\lambda_n X) - Y_1(\lambda_n)J_0(\lambda_n X)\right]e^{-\lambda_n^2 t} + \frac{k_2X^2}{4} - \left(\delta + \frac{k_2}{2}\right)\ln(X) + k_2\tau + a_2, \quad \alpha < X \le 1 \quad [57]$$

Here $J_\alpha(.)$ and $Y_\alpha(.)$ are the Bessel functions of first and second kind respectively. The eigenvalues are the positive roots of following equation

$$\beta^2\chi_2^c J_0(\theta_n) + \chi_1^c\left(\beta^2\kappa\lambda_n\left[Y_1(\lambda_n)J_0(\lambda_n\alpha) - J_1(\lambda_n)Y_0(\lambda_n\alpha)\right] + \frac{\beta\lambda\chi^2}{\gamma}\right) = 0 \quad [58]$$

where $\theta_n = \alpha\lambda_n\beta$. The summation coefficient is given as

$$A_n = \frac{2J_1(\theta_n)\delta\kappa}{\lambda_n^2\pi\left(\frac{(\chi_1^c)^2\alpha^2}{2}\left[J_0^2(\theta_n) + J_1^2(\theta_n)\right] + J_1^2(\theta_n)\lambda_n^2\kappa\left[\chi_2^cY_1^2(\lambda_n) + \chi_4^cJ_1(\lambda_n)Y_1(\lambda_n) + \chi_3^cJ_1^2(\lambda_n)\right]\right)} \quad [59]$$

where

$$\chi_1^c = \beta\lambda_n\left[Y_1(\lambda_n\alpha)J_1(\lambda_n) - J_1(\lambda_n\alpha)Y_1(\lambda_n)\right] \quad [60]$$

$$\chi_2^c = \frac{1}{2}\left[J_0^2(\lambda_n) - \alpha^2\left(J_1^2(\lambda_n\alpha) + J_0^2(\lambda_n\alpha)\right)\right] \quad [61]$$

$$\chi_3^c = \frac{1}{2}\left[Y_0^2(\lambda_n) - \alpha^2\left(Y_1^2(\lambda_n\alpha) + Y_0^2(\lambda_n\alpha)\right)\right] \quad [62]$$

$$\chi_4^c = \alpha^2\left[Y_0(\lambda_n\alpha)J_0(\lambda_n\alpha) + J_1(\lambda_n\alpha)Y_1(\lambda_n\alpha)\right] - Y_0(\lambda_n)J_0(\lambda_n) \quad [63]$$

and the constants are given as

$$k_1 = \kappa k_2 = \frac{-2\kappa\delta}{\alpha^2(\kappa-1)+1} \quad [64]$$

$$a_1 = \frac{\left[4\alpha^2(1-\kappa)\ln(\alpha) - \left(\beta^2(2-\kappa)+1-2\kappa\right)\alpha^4 + \left(\beta^2-\kappa\right)2\alpha^2 + 1\right]\delta\kappa}{4\left(\alpha^2(\kappa-1)+1\right)^2} + \frac{\left(\alpha^2-1\right)\alpha\delta\kappa}{\left(\alpha^2(\kappa-1)+1\right)^2\gamma} \quad [65]$$

$$a_2 = \frac{a_1}{\kappa} + \frac{\delta\alpha}{2}\left[\frac{2}{\gamma\left(\alpha^2(\kappa-1)+1\right)} + \frac{\left[(\kappa-1)2\alpha\ln(\alpha) + \alpha\left(1-\beta^2\right)\right]}{\left(\alpha^2(\kappa-1)+1\right)}\right] \quad [66]$$

Spherical geometry.— As described in detail for the rectangular core-shell, one can derive the solution for isotropic radial diffusion for spherical composite particle. For spherical system the governing equations are

$$\frac{\partial}{\partial\tau}x_1(X,\tau) = \frac{1}{\beta^2}\frac{1}{X^2}\frac{\partial}{\partial X}\left(X^2\frac{\partial}{\partial X}x_1(X,\tau)\right), \quad 0 < X < \alpha \quad [67]$$

$$\frac{\partial}{\partial\tau}x_2(X,\tau) = \frac{1}{X^2}\frac{\partial}{\partial X}\left(X^2\frac{\partial}{\partial X}x_1(X,\tau)\right), \quad \alpha < X < 1 \quad [68]$$

The initial and boundary conditions can be expressed using Eqs 6, 7, 8, 9, and 10. The solution for spherical geometry can be derived as

$$x_1(X,\tau) = \sum_{n=1}^{\infty} -A_n\frac{\chi_2^s\beta^2}{\lambda_n}\left(\frac{\sin(\lambda_n\beta X)}{X}\right)e^{-\lambda_n^2\tau} + \frac{1}{6}k_1\beta^2X^2 + k_1\tau + a_1, \quad 0 \le X < \alpha \quad [69]$$

$$x_2(X,\tau) = \sum_{n=1}^{\infty} -A_n\frac{\chi_1^s}{\lambda_n}\left(\frac{\lambda_n\cos[\lambda_n(X-1)] + \sin[\lambda_n(X-1)]}{X}\right) \times e^{-\lambda_n^2\tau} + \frac{1}{6}k_2X^2 + \frac{1}{X}\left(\delta + \frac{1}{3}k_2\right) + k_2\tau + a_2, \quad \alpha < X \le 1 \quad [70]$$

where eigenvalues are the roots of following equation (using $\theta_n = \alpha\lambda_n\beta$, and $\phi_n = \lambda_n(\alpha - 1)$).

$$\left(\theta_n^2 - \frac{\theta_n^2}{\lambda_n \tan\phi_n}\right) + \left(\alpha + \frac{\alpha\lambda_n}{\tan\phi_n}\right)\left(\beta^2 - \kappa + \frac{\theta_n\kappa}{\tan\theta_n}\right) + \frac{1}{\gamma}\left(1 - \frac{\theta_n}{\tan\theta_n}\right)\left(\alpha\lambda_n^2 + 1 - \frac{\phi_n}{\tan\phi_n}\right) = 0 \quad [71]$$

The summation coefficients are given as follows:

$$A_n = \frac{2\chi_1^s\delta\kappa\lambda_n}{\left[\beta^3\left(\chi_2^s\right)^2\chi_3^s - \chi_4^s\left(\chi_1^s\right)^2\kappa\right]} \quad [72]$$

where the constituents are given as

$$\chi_1^s = \theta_n\cos\theta_n - \sin\theta_n \quad [73]$$

$$\chi_2^s = \phi_n\cos\phi_n - \left(\alpha\lambda_n^2 + 1\right)\sin\phi_n \quad [74]$$

$$\chi_3^s = \cos\theta_n\sin\theta_n - \theta_n \quad [75]$$

$$\chi_4^s = \left(1 - \lambda_n^2\right)\cos\phi_n\sin\phi_n + 2\lambda_n\cos^2\phi_n - \phi_n\lambda_n^2 - (\alpha + 1)\lambda_n \quad [76]$$

and values of constants (a_1, a_2, k_1, and k_2) in this case turn out to be

$$k_1 = \kappa k_2 = \frac{-3\kappa\delta}{\alpha^3(\kappa - 1) + 1} \quad [77]$$

Cases with $\kappa < 1$ are similar to diffusion in a sphere with single domain as the inner core will always have lower concnetration than the outer core. But interesting stress profiles can be seen in these cases depending on the values of partial molar volume (Ω). For example, three cases can be visualized for $\Omega_{core}/\Omega_{shell} < \kappa$, $\Omega_{core}/\Omega_{shell} = \kappa$, $\Omega_{core}/\Omega_{shell} > \kappa$ that will generate different stress profiles.

Next, we demonstrate the use of derived solution to describe diffusion in special cases. For example, choice of $\kappa \ll 1$ can mimic the transport of lithium in hollow spherical particle or particle with inert core, Figure 6 shows the concentration profiles in a hollow sphere using $\kappa = 10^{-10}$, and $\beta = 10^{-4}$.

Similarly, using $\kappa = 2$, $\beta = 1$, $\gamma \gg 1$, the solution derived by Subramanian and White[8] can be constructed (Figure 7) suggesting the validity and flexibility of the model developed. Lastly, using $\kappa = 1$, $\beta = 1$, and $\gamma \gg 1$, solution for diffusion in a sphere with single domain can be obtained (Figure 8). The model developed shows that while very little changes may be observed in the charge discharge curves (qualitatively), situation deep inside the core shell material can be very different from the spherical particle case with the same material.

Application in Stress Estimation in Core-Shell Composite Particles

One of the reasons for designing core-shell type composite electrode materials is to circumvent the pulverization of high energy materials with high volumetric expansion. Intercalation induced stress generation is one of the main reasons for capacity fade. Models to quantify intercalation-induced stress can be divided into two categories: strain splitting[12,14–16] and stress splitting.[18,19] The theory of the strain splitting approach has been developed by Timoshenko[20] where thermal stresses have been modeled using strain splitting, with these models being called *thermal analogy models*. Here, the intercalation-induced stresses are treated in similar way as the temperature-induced stresses. A very detailed model that used stress splitting was developed by Christensen et al.,[18,19] which was shown to be equivalent to the former approach (strain splitting) by Timoshenko.[20] In both categories, different models can be obtained depending upon the inclusion of pressure-induced diffusion. Inclusion of pressure induced diffusion results in nonlinear partial differential equations (PDEs). It is very difficult to apply analytical treatment to such PDEs, hence this paper focuses on stress calculation ignoring pressure induced diffusion and using strain splitting method. Detailed description of strain-splitting method to model intercalation induced stresses in spherical geometry with isotropic radial diffusion can be found in literature.[12,14–16] Deshpande et al.[14] presented analytical expressions for the intercalation-induced stresses developed in a spherical particle with moving phase boundary assuming lithium concentration independent material properties (Young's modulus (E), partial molar volume (Ω), Poisson's ratio (ν)) and neglecting volume expansion. These assumptions may not give accurate description for systems with high volume expansion (e.g. Silicon), but they allow analytical treatment of the problem and decouple concentration and stresses. Expressions are listed in dimensionless form for radial (σ_r) and tangential stresses (σ_t) in both regions of the isotropic spherical particle with only radial diffusion, derivation of these equations can

$$a_1 = \frac{\left[\left(\left(-3\beta^2 - 5\right)\alpha^5 + 15\alpha^3 - 10\alpha^2\right)(1 - \kappa) + \left(1 - \beta^2\right)\left(2\alpha^3 + 5\right)\alpha^2 + 3\right]\delta\kappa}{10\left[\alpha^3(\kappa - 1) + 1\right]^2} + \frac{\left(\alpha^3 - 1\right)\alpha\delta\kappa}{\left[\alpha^3(\kappa - 1) + 1\right]^2\gamma} \quad [78]$$

$$a_2 = -\frac{\left[10\alpha^5(1 - \kappa)^2 + \left(\left(-2\beta^2 + 10\right)\alpha^5 - 15\alpha^3\right)(1 - \kappa) - \left(1 - \beta^2\right)2\alpha^5 - 3\right]\delta}{10\left[\alpha^3(\kappa - 1) + 1\right]^2} + \frac{\kappa\alpha^4\delta}{\left[\alpha^3(\kappa - 1) + 1\right]^2\gamma} \quad [79]$$

Results

This section presents transient concentration profiles for spherical core-shell particle. Though the solution is general enough to describe slower interfacial dynamics, for illustration purposes, only cases with very fast interfacial kinetics ($\gamma \gg 1$) are discussed. Three different sets of parameter values are chosen to visualize the diffusion dynamics that resemble to cases B, C and D in Figure 2.

Figure 3 presents concentration profiles for $\beta > 1$ and $\kappa > 1$ (equivalent to case C in Figure 2). For $\kappa = 2$, the interfacial concentration in the core will be twice compared to the interfacial concentration in the shell. Moreover two orders of magnitude difference in diffusivity ($\beta^2 = D_2/D_1 = 100$) will create steep concentration gradients in the core which will lead to significant stress development in the particle. The initial concentration at t = 0 (Gibb's Phenomena), is also shown in following Figs. 3–8.

Figure 4 describes the concentration profiles for $\beta = 1$ and $\kappa > 1$ (close to case D in Figure 2). The choice of above parameters leads to interesting situation of having the inner core more concentrated than the shell. This situation can never occur in single domain spherical charging with nonnegative current. One interesting difference in the current case versus the previous case is that despite having κ greater than one, the average concentration in inner core is smaller than the shell for the previous case. This phenomenon will alter the stress dynamics discussed in the following section.

Figure 5 describes the concentration profiles for $\beta < 1$ and $\kappa < 1$ (equivalent to case B in Figure 2). As the inner core has higher diffusion coefficient than the outer shell, a flat concentration profile is expected in the inner core.

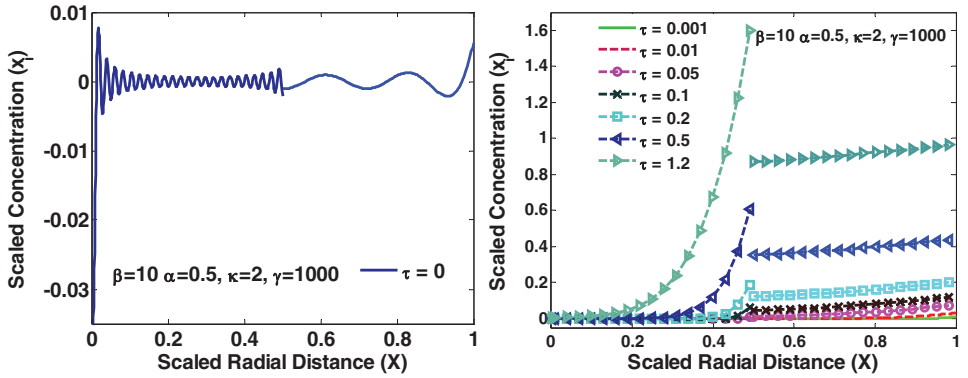

Figure 3. (Left) concentration at t = 0, (Right) concentration profiles during intercalation.

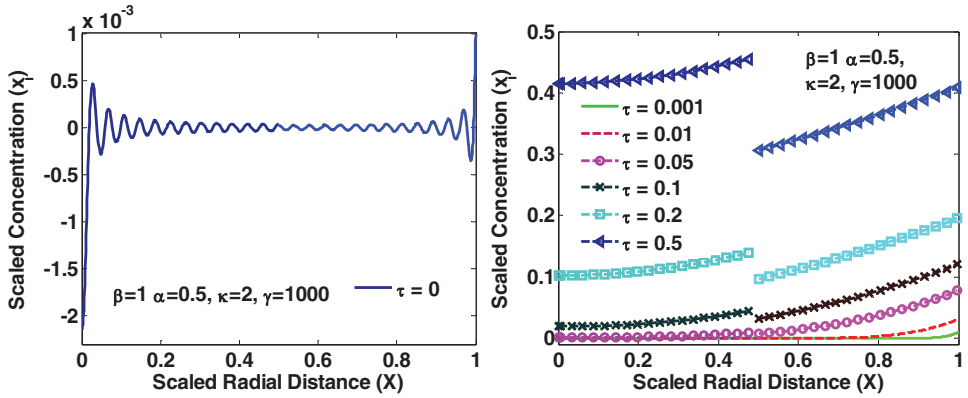

Figure 4. (Left) concentration at t = 0, (Right) concentration profiles during intercalation at different time.

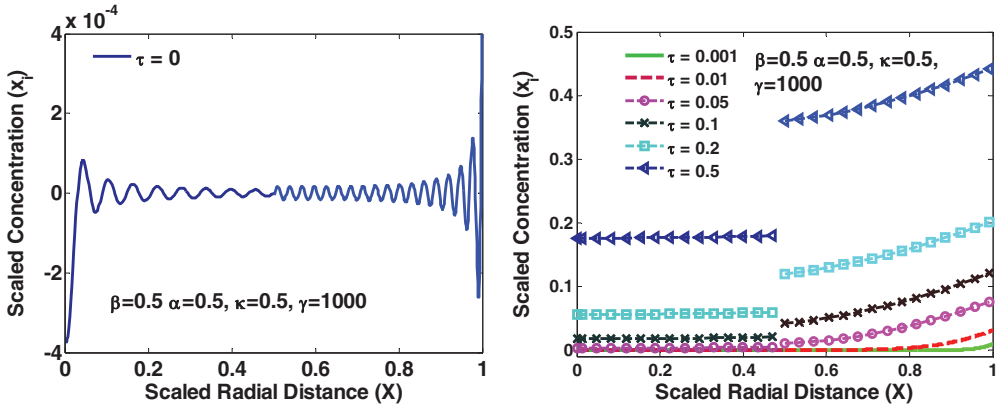

Figure 5. (Left) concentration at t = 0, (Right) concentration profiles during intercalation at different time.

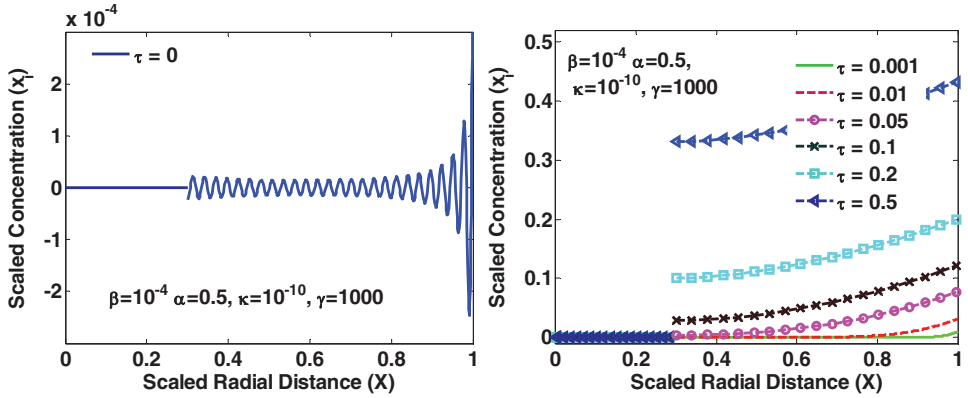

Figure 6. (Left) concentration profiles at t = 0, (Right) concentration profiles during intercalation at different time in a hollow sphere (inert core).

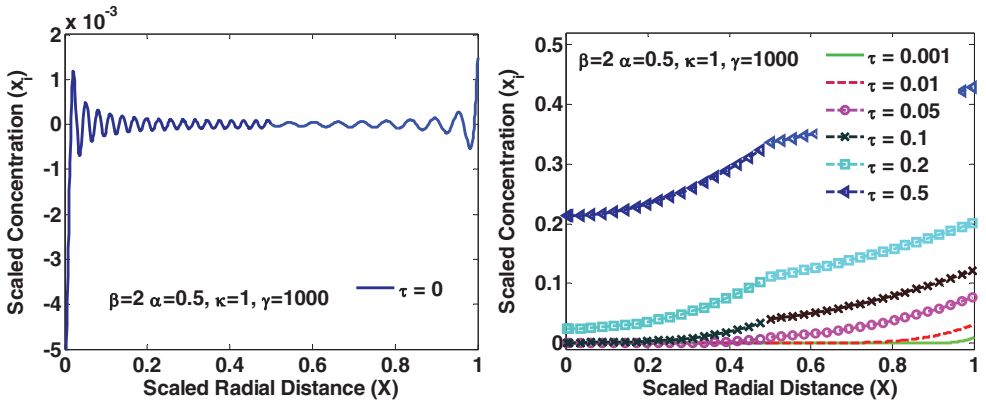

Figure 7. (Left) concentration at t = 0, (Right) concentration profiles during intercalation at different time in sphere with continuous concentration at the interface.

be found in Deshpande et al.[14] Defining following expressions

$$Q_1(X) = \int_0^X \xi^2 x_1(\xi)\, d\xi \qquad [80]$$

$$Q_2(X) = \int_\alpha^X \xi^2 x_2(\xi)\, d\xi \qquad [81]$$

where ξ is a dummy integration variable, $x_i = c_i/c_0$ and introducing the dimensionless variables

$$\hat{\sigma}_{r_i} = \frac{\sigma_{r_i}}{\sum}; \hat{\sigma}_{t_i} = \frac{\sigma_{t_i}}{\sum} \qquad [82]$$

where $\sum = c_0\Omega_2 E_2$ and dimensionless parameters

$$\Theta = \frac{E_1}{E_2}; \Pi = \frac{\Omega_1}{\Omega_2} \qquad [83]$$

the dimensionless radial and tangential stress can be expressed as

$$\widehat{\sigma}_{r_1}(X) = \frac{2}{3}\frac{\Pi\Theta}{(1-\nu_1)}\left(\frac{\Delta_2}{\alpha^3\Delta_1}Q_1(\alpha) - \frac{1}{X^3}Q_1(X) - \frac{3(1-\nu_1)}{\Delta_1\Pi}Q_2(1)\right), \quad 0 < X < \alpha \qquad [84]$$

$$\widehat{\sigma}_{t_1}(X) = \frac{2}{3}\frac{\Pi\Theta}{(1-\nu_1)}\left(\frac{\Delta_2}{\alpha^3\Delta_1}Q_1(\alpha) - \frac{3(1-\nu_1)}{\Pi\Delta_1}Q_2(1) + \frac{1}{2}\frac{Q_1(X)}{X^3} - \frac{1}{2}x_1(X)\right), \quad 0 < X < \alpha \qquad [85]$$

$$\widehat{\sigma}_{r_2}(X) = \frac{2}{3(1-\nu_2)}\left(\frac{3\Theta\Pi\left(1-X^3\right)(1-\nu_2)}{\Delta_1 X^3}Q_1(\alpha) + \left(\frac{2\alpha^3\Delta_3}{\Delta_1 X^3} - \frac{\Delta_4}{\Delta_1}\right)Q_2(1) - \frac{Q_2(X)}{X^3}\right), \quad \alpha < X < 1 \qquad [86]$$

$$\widehat{\sigma}_{t_2}(X) = \frac{1}{(1-\nu_2)}\left(\frac{Q_2(X)}{3X^3} - \frac{x_2(X)}{3} - \frac{\Theta\Pi(1-\nu_2)}{\Delta_1}\left(2+\frac{1}{X^3}\right) \times Q_1(\alpha) - \left(\Delta_4 + \frac{\Delta_3\alpha^3}{X^3}\right)\frac{2Q_2(1)}{3\Delta_1}\right), \quad \alpha < X < 1 \qquad [87]$$

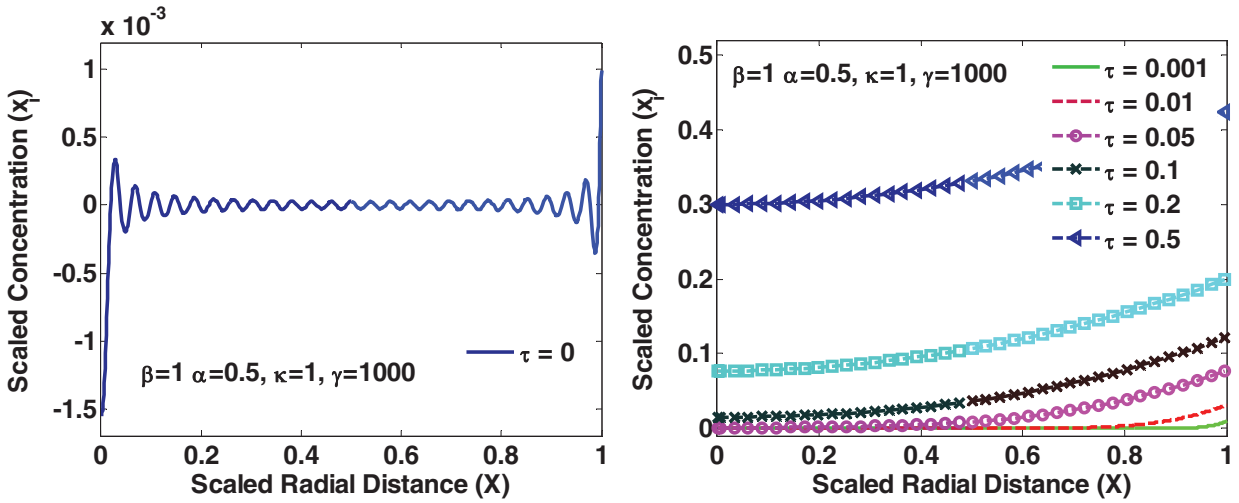

Figure 8. (Left) concentration at t = 0, (Right) concentration profiles during intercalation at different time with core and shell having exact same material properties.

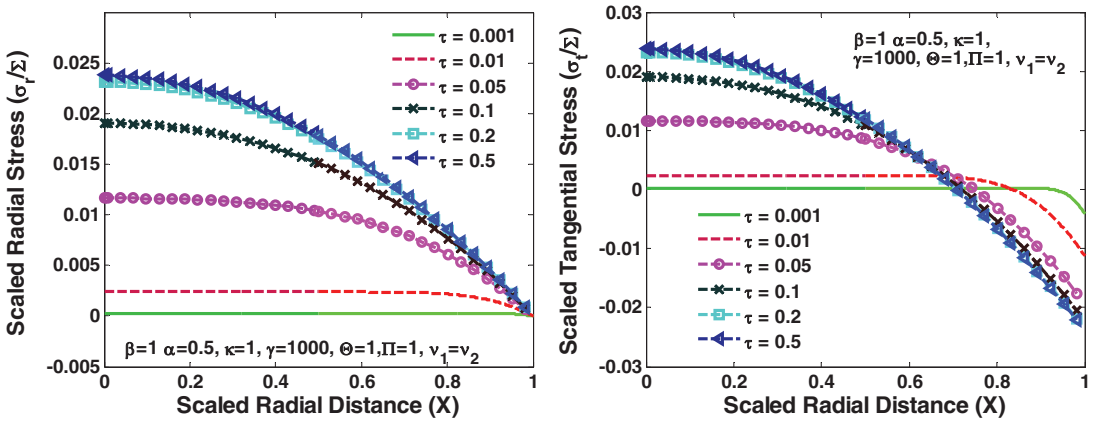

Figure 9. Radial and tangential stresses during galvanostatic intercalation in spherical particle of single domain.

where

$$\Delta_0=[2(2\nu_2-1)\alpha^3-(1+\nu_2)]\Theta, \quad \Delta_1=\Delta_0+2(1-\alpha^3)(2\nu_1-1),$$

$$\Delta_2=\Delta_0+(1-\alpha^3)(1+\nu_1), \quad \Delta_3=(2\nu_2-1)\Theta+1-2\nu_1,$$

$$\text{and } \Delta_4=(1+\nu_2)\Theta+2(1-2\nu_1) \qquad [87]$$

Three scenarios are discussed using $\delta=-0.25$. First, a core-shell particle with continuous concentration profiles using $\kappa=1$, and $\gamma\gg1$ is considered (Figure 7 and Figure 8). Then, stress generation in core-shell particles with discontinuous concentration (specifically $\kappa>1$) are presented (Figure 3 and Figure 4) followed by hollow sphere (Figure 6).

Core-shell sphere with continuous concentration at the interface ($\kappa=1$, $\gamma\gg1$).— If transport and mechanical properties of both the regions are taken equal with fast interfacial dynamics (i.e. $\kappa=1$, $\beta=1$, $\Pi=1$, $\Theta=1$, and $\nu_1=\nu_2$), the resultant configuration will denote diffusion and stress generated in a sphere with single domain. Figure 8 shows the concentration distribution and Figure 9 shows the radial and tangential stresses. Simplification of this magnitude gives rise to the basic understanding of intercalation induced stresses in a particle. The radial and tangential stresses are mainly dependent on some representation of the gradient of concentration profiles (difference between average concentration up to the point of interest and total average concentration). As the short time dynamics start to fade out (around $\tau=0.2$ in Figure 8), the stress profiles start to saturate reaching a maxima (Figure 9), which is expected as the steepness of profiles remains constant afterwards. Positive values of stress represent tensile stress and negative values denote compressive stress. The concentration profiles make the outer layers expand more compared to inner layers resulting in tensile radial stress during intercalation at every point in *X*. Tangential stresses on the other hand are compressive at the surface and tensile at the center. The peak compressive stress occurs at the surface and peak tensile stress at the center of the particle and the locations for peak stresses do not change during intercalation.

Saturation of stresses to a maximum value is due to uniform partial molar volume for both materials. If partial molar volume of the inner core is assumed to be larger than the outer shell (i.e. $\Pi>1$) keeping other parameters same, the stress profiles will change drastically even though the concentration profiles will remain the same. After the short time dynamics die out, the inner core will have to face more expansion due to higher partial molar volume facing resistance from the shell while expanding, which will result in compressive nature of radial and tangential stresses at the center. As can be seen from Figure 10, the peak radial and tangential stresses at the center go through a maxima and then change from tensile to compressive. Location and nature of peak stresses for the inner core also changes from the center to the interface and from tensile to compressive.

Similarly, if the partial molar volume of the core is small compared to the shell (i.e. $\Pi<1$), the radial stress will remain positive (tensile stress) at every point in *X* and keep increasing. Tangential stress in the core will also remain positive but at the interface, it will go through a maxima and then change from tensile to compressive.

Though having different values of diffusivity in both regions ($\beta\neq1$) will affect the magnitude of stress developed as steepness of concentration profiles is affected by the values of β (Figure 7), the shape of underlying profiles remains more or less similar.

Core-shell sphere with discontinuous concentration at the interface ($\kappa\neq1$, $\gamma\gg1$).— The parameters in this section are chosen

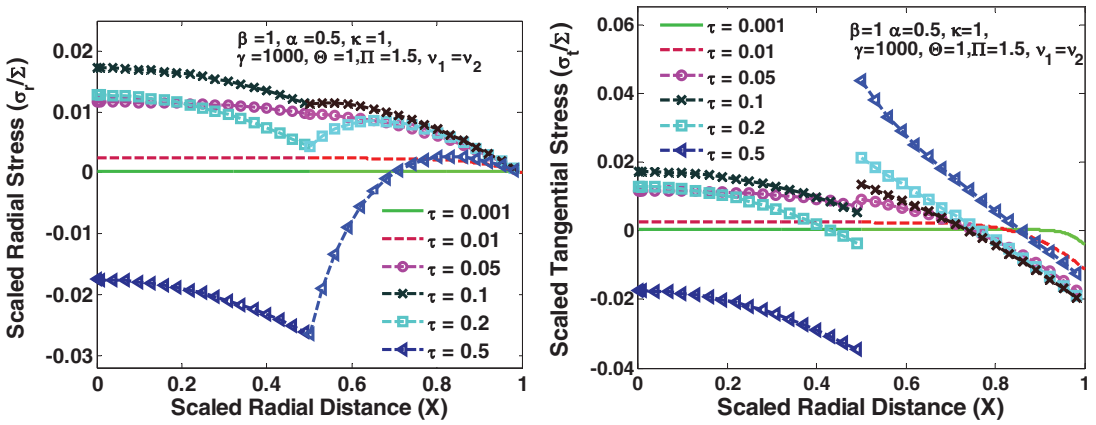

Figure 10. Radial and tangential stresses during galvanostatic intercalation in spherical particle with higher partial molar volume for the core.

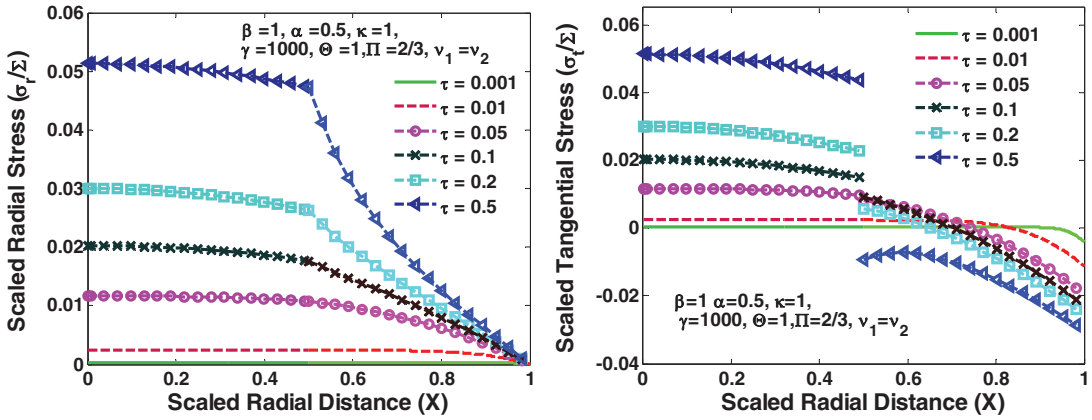

Figure 11. Radial and tangential stresses during galvanostatic intercalation in spherical particle with lower partial molar volume for the core.

to represent a core-shell configuration where the core comprises of higher capacity material. The diffusion coefficient of the inner core is assumed to be two orders of magnitude smaller than that of the outer shell ($\beta^2 = D_2/D_1 = 100$) and Young's modulus of the core is assumed to be one order of magnitude larger than the shell ($\Theta = \Omega_1/\Omega_2 = 10$). Values of other parameters, κ and Π are taken as 2 and 1.5. As the inner core has higher magnitudes of stresses compared to the outer shell, a different kind of scaling ($\text{sgn}[(\cdot)]\,|(\cdot)|^{1/4}$, here sgn is a signum function) is done to represent the stresses in Figure 12. This scaling takes care of both positive and negative values and maintains continuity of radial stresses (also the reason for the amplification in the Gibb's phenomenon). As the diffusivity of the core is very small compared to the shell, more time is required for transient behavior to fade out hence stress profiles are plotted up to $\tau = 1.2$.

In this configuration, the radial and tangential stresses at the center keep rising and remain tensile for all time. This is due to very small diffusion coefficient in the core compared to the shell which, in effect, restricts the core to have enough concentration that can swell the core despite higher partial molar volume and higher interfacial concentration. Even though the concentration in the core is small compared to the shell, the interface on the core side will have double the concentration and partial molar volume compared to the interface on the shell side. This causes the core side interface to swell significantly compared to its nearby region, developing compressive stress at the interface ($\tau = 1.2$ in Figure 12).

If the ratio of diffusivity (β^2) is changed to 1 keeping other parameters constant, that will make the core more concentrated than the shell (after the short time transient dies out, Figure 4), in that case expansion of the core aided with higher partial molar volume will lead to compressive radial and tangential stresses in the core (Figure 13).

The magnitude of peak stresses in the particle also depends on the ratio of core and shell thicknesses (α). As the thickness of the core (high energy density material) is decreased, stress generated will be smaller due to flatter concentration profiles in the core (less diffusion resistance). This situation conflicts with the objective of having increased energy density compared to graphite particle. On the other hand, if the value of α is chosen close to 1, the stress generated will be significantly higher, which may lead to breaking of the outer shell. Hence a careful selection of material properties is needed in order to deliver efficient energy storage material. As seen earlier, changes in one or two parameters can drastically change the stress behavior which gives an opportunity to carefully tune the transport parameters for better material properties to address issues relating to capacity fade. Our future efforts will address optimization of these design parameters based on the model reported here.

Hollow sphere or sphere with inert core.— As discussed earlier (Figure 6), solution derived in this paper can be used to mimic the transport behavior of a hollow spherical particle or a particle with inert core. Stress profile for the same is plotted in Figure 14. Absence of the inner core will result in the absence of radial stresses at the inner surface of the particle. This can equivalently be represented as very small Young's modulus for the core ($\Theta = 10^{-10}$) with equal partial molar volume ($\Pi = 1$). Following plots were obtained by choosing α

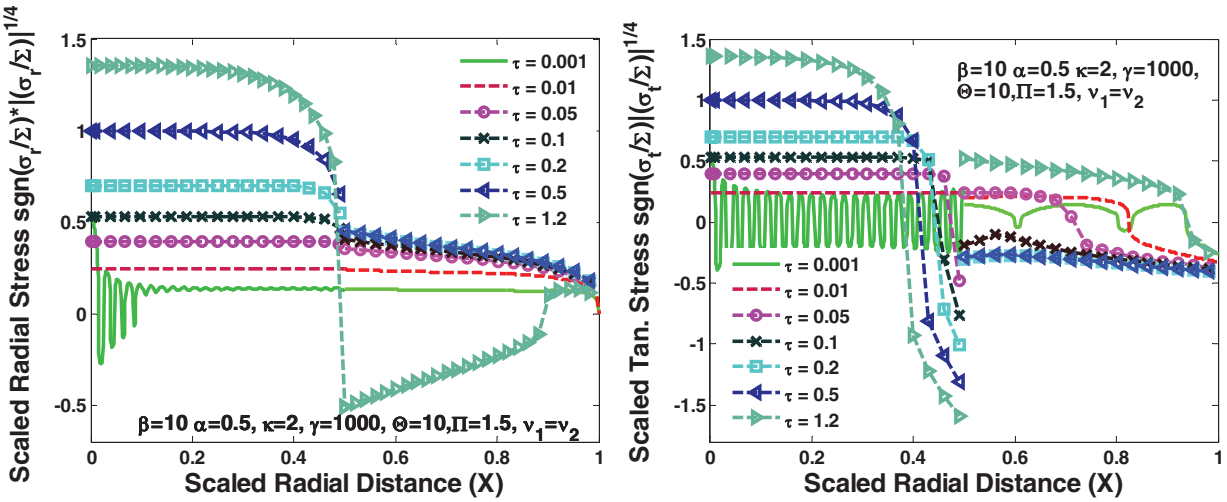

Figure 12. Radial and tangential stresses during galvanostatic intercalation in Si/C type core-shell particle; oscillations are amplified due to scaling.

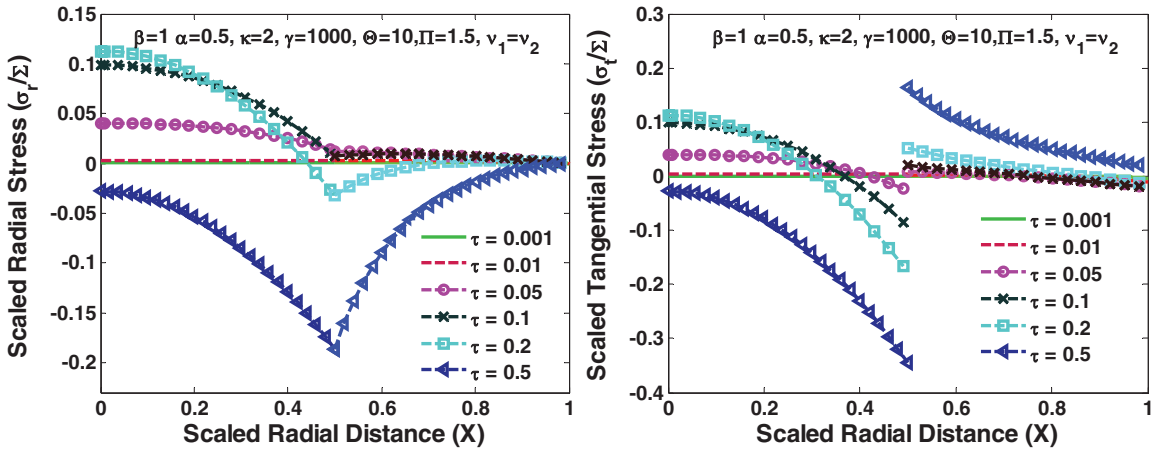

Figure 13. Radial and tangential stresses during galvanostatic intercalation in Si/C type core-shell particle for equal diffusivities.

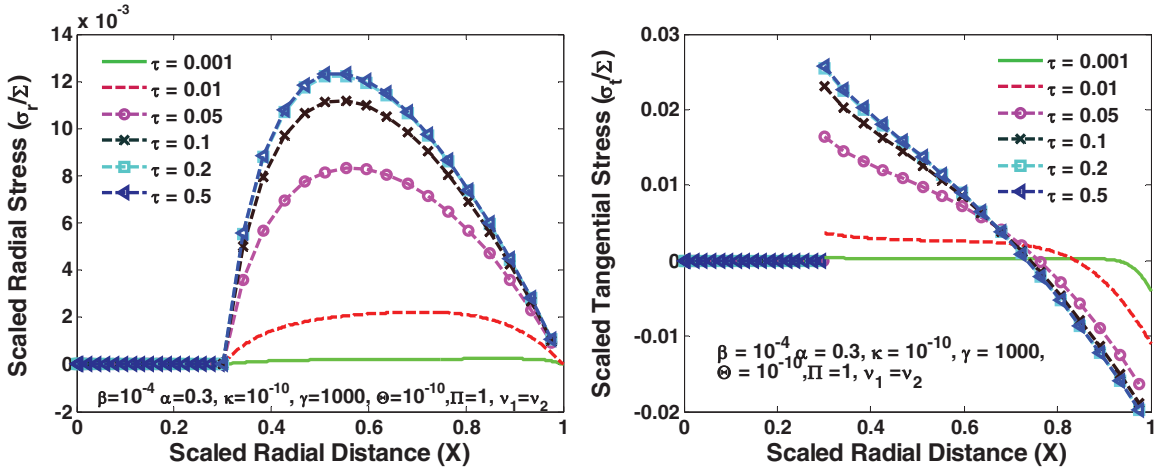

Figure 14. Radial and tangential stresses for hollow sphere.

$= 0.3, \delta = -0.25$, $\nu_1 = 0.3$, and $\nu_2 = 0.3$. As the radial stress is zero on both the surfaces, the radial stress in the particle goes through a maxima for $\alpha < X < 1$. Moreover, the peak radial stress and tangential stress saturate to a maximum value for large τ. Figure 14 also shows that the location of peak radial stress shifts toward the center from surface under these charging conditions.

Similar stress calculations can be performed for radial isotropic diffusion in core-shell and hollow cylindrical geometry. The above analysis does not incorporate volume expansion, pressure induced diffusion and concentration dependent material properties. As there can exist a significant stress difference at the interface (Figure 10, Figure 11, Figure 12, and Figure 13), pressure induced diffusion may play a significant role and alter the dynamics.

Code Dissemination

In order to facilitate the use of derived solution considering the complexity of the expressions, final analytical expressions for concentration profiles for three geometries in MAPLE and MATLAB environments will be hosted at the authors' website.[21] In addition, a code to calculate radial and tangential stresses in spherical core-shell particle according to model used in the paper will also be hosted on the website.

Conclusions

Intercalation of lithium in core-shell material is modeled with a very general treatment at the interface including interfacial dynamics. The model is solved using a modified separation of variables method developed earlier. It was shown that diffusion in core-shell particles can be modeled using 3 important parameters (ratio of diffusivities, ratio of equilibrium concentrations, and interface dynamics). Cases studied in this paper assumes very fast interfacial dynamics but slower interfacial dynamics do play a role in concentration profiles and stress behavior specially at short times.

In addition, we plan to perform (1) Efficient reformulation[22,23] for particle level dynamics in core-shell model for faster simulation. (1) Reformulated Pseudo 2D model[24] using the core-shell model at the particle level. (3) Model based design of material properties,[25,26] both at the particle level and sandwich level of lithium ion batteries. (4) Derivation of optimal charging profiles using reformulated models to reduce capacity fade.[27,28] (5) Identification of transport parameters using impedance response of core-shell materials from experimental data.

Acknowledgments

This paper is based upon work supported in part under the US-India Partnership to Advance Clean Energy-Research (PACE-R) for the Solar Energy Research Institute for India and the United States (SERIIUS), funded jointly by the U.S. Department of Energy (Office of Science, Office of Basic Energy Sciences, and Energy Efficiency and Renewable Energy, Solar Energy Technology Program, under Subcontract DE-AC36-08GO28308 to the National Renewable Energy Laboratory, Golden, Colorado) and the Government of India, through the Department of Science and Technology under Subcontract

IUSSTF/JCERDC-SERIIUS/2012 dated 22nd Nov. 2012. The authors are also thankful for the financial support from the United States Government, Advanced Research Projects Agency–Energy (ARPA-E), U.S. Department of Energy, under award number DE-AR0000275, and McDonnell International Scholar Academy at Washington University in St. Louis.

List of Symbols

A_n	Coefficients in infinite series
a_i, k_i	Constants used to represent solution
α	Fractional coverage of region 1 (R_1/R_2)
B_i	Constants
β^2	Ratio of diffusivity (D_2/D_1)
c_i^*	Equilibrium concentration, mol/m3
c_i^*	Concentration, mol/m3
χ_m^j	Eigenvalues dependent constants
D_i	Diffusion coefficient, m^2/s
Δ_i	Dimensionless groups to represent stress in compact form
δ	Dimensionless current density
E	Young's modulus, Pa
F	Faraday's constant, 96487 C/g equivalent
$f_i(X)$	Eigenfunctions
ϕ_n, θ_n	Eigenvalues dependent constants
g_i	Variable to present Homogeneous solution
γ	Dimensionless interfacial kinetics
I_s	Current density, A/m^2
κ	Ratio of equilibrium concentration
ℓ	Interfacial dynamics, m/s
λ_i	Constant
λ_n	Eigenvalues
N_i	Molar flux, $mol/s/m^2$
n	Charge associated with the single ion of guest molecule
Π	Ratio of partial molar volume
Θ	Ratio of Young's Modulus
r	Axial distance/radial distance, m
R_1	Thickness of first region, m
R_2	Total thickness of the geometry, m
σ_{r_i}	Radial stress, Pa
σ_{t_i}	Tangential stress, Pa
$\hat{\sigma}_{r_i}$	Dimensionless radial stress
$\hat{\sigma}_{t_i}$	Dimensionless tangential stress
t	Time, sec
τ	Dimensionless time
ν	Poisson's ratio
w_i, v_i,	Variables to present nonhomogeneous solution
x_i	Dimensionless concentration
X	Dimensionless axial/radial distance
Ω	Partial molar volume, m^3/mol

Subscripts Used in List of Symbols

i	$i = 1$ *or* 2, for region 1 ($0 < r < R_1$) and region 2 ($R_1 < r < R_2$)
n	$n = 1..\infty$, positive eigenvalues
m	Constants used to make the expression compact (used in χ_m^j)

List of Superscript

p, c, s	Denote planar, cylinder and sphere respectively (used in χ_m^j)

References

1. C. Daniel, *JOM Journal of the Minerals, Metals and Materials Society*, **60**, 43 (2008).
2. S. M. Lukic, J. Cao, R. C. Bansal, F. Rodriguez, and A. Emadi, *Ieee Transactions on Industrial Electronics*, **55**, 2258 (2008).
3. V. Pop, H. J. Bergveld, D. Danilov, P. P. L. Regtien, and P. H. L. Notten, *Battery Management Systems: Accurate State-of-Charge Indication for Battery Powered Applications*, Springer, Dordrecht (2008).
4. M. M. Ren, Z. Zhou, X. P. Gao, W. X. Peng, and J. P. Wei, *The Journal of Physical Chemistry C*, **112**, 5689 (2008).
5. A. M. Wilson and J. R. Dahn, *J. Electrochem. Soc.*, **142**, 326 (1995).
6. A. S. Arico, P. Bruce, B. Scrosati, J.-M. Tarascon, and W. van Schalkwijk, *Nat Mater*, **4**, 366 (2005).
7. F. M. Hassan, V. Chabot, A. R. Elsayed, X. Xiao, and Z. Chen, *Nano Letters* (2013).
8. V. R. Subramanian and R. E. White, *Journal of Power Sources*, **96**, 385 (2001).
9. H. Carslaw and J. Jaeger, *Conduction of Heat in Solids*, Oxford University Press, London (1973).
10. G. Pontrelli and F. de Monte, *International Journal of Heat and Mass Transfer*, **50**, 3658 (2007).
11. G. Pontrelli and F. de Monte, *International Journal of Heat and Mass Transfer*, **53**, 3629 (2010).
12. Y.-T. Cheng and M. W. Verbrugge, *Journal of Power Sources*, **190**, 453 (2009).
13. R. Deshpande, Y.-T. Cheng, and M. W. Verbrugge, *Journal of Power Sources*, **195**, 5081 (2010).
14. R. Deshpande, Y.-T. Cheng, M. W. Verbrugge, and A. Timmons, *J. Electrochem. Soc.*, **158**, A718 (2011).
15. X. Zhang, W. Shyy, and A. Marie Sastry, *J. Electrochem. Soc.*, **154**, A910 (2007).
16. S. Renganathan, G. Sikha, S. Santhanagopalan, and R. E. White, *J. Electrochem. Soc.*, **157**, A155 (2010).
17. C. W. Tittle, *J Appl Phys*, **36**, 1486 (1965).
18. J. Christensen and J. Newman, *J Solid State Electr*, **10**, 293 (2006).
19. J. Christensen and J. Newman, *J. Electrochem. Soc.*, **153**, A1019 (2006).
20. S. Timoshenko, *Theory of elasticity, section 107*, McGraw Hill Book Company, New York (1934).
21. M. A. P. L. E. Website, [http://www.maple.eece.wustl.edu/, last accessed Mar 2014]
22. S. De, B. Suthar, D. Rife, G. Sikha, and V. R. Subramanian, *J. Electrochem. Soc.*, **160**, A1675 (2013).
23. V. Ramadesigan, V. Boovaragavan, J. C. Pirkle, and V. R. Subramanian, *J. Electrochem. Soc.*, **157**, A854 (2010).
24. P. W. C. Northrop, V. Ramadesigan, S. De, and V. R. Subramanian, *J. Electrochem. Soc.*, **158**, A1461 (2011).
25. V. Ramadesigan, P. W. C. Northrop, S. De, S. Santhanagopalan, R. D. Braatz, and V. R. Subramanian, *J. Electrochem. Soc.*, **159**, R31 (2012).
26. D. Sumitava, P. W. Northrop, V. Ramadesigan, and V. R. Subramanian, *Journal of Power Sources* (2012).
27. B. Suthar, V. Ramadesigan, S. De, R. D. Braatz, and V. R. Subramanian, *Physical Chemistry Chemical Physics*, **16**, 277 (2014).
28. B. Suthar, V. Ramadesigan, P. W. C. Northrop, B. Gopaluni, S. Santhanagopalan, R. D. Braatz, and V. R. Subramanian, in *American Control Conference (ACC), 2013*, p. 5350.